The Decarboxylation and Protonation Enigma in the H85Q Mutant of Cytochrome $P450_{OleT}$

Shalini Yadav, Sason Shaik*, and Kshatresh Dutta Dubey*

1. Department of Chemistry, School of Natural Science, Shiv Nadar Institution of Eminence, NH91 Tehsil Dadri, Greater Noida, Uttar Pradesh 201314, India. kshatresh.dubey@snu.edu.in
2. Institute of Chemistry, Edmond J. Safra Campus at Givat Ram, The Hebrew University, Jerusalem, 9190401 Israel. sason@yfaat.ch.huji.ac.il

Abstract: Cytochrome $P450_{OleT}$ ($CYP450_{OleT}$), a member of CYP450 Peroxygenases, catalyzes unusual decarboxylation activity. Unlike other members of the peroxygenases family, $CYP450_{OleT}$ possesses a Histidine at the 85th position, which was supposed to be the root cause of the decarboxylation activity in $CYP450_{OleT}$. *This work addresses the His85→Gln mutant paradox where mutation of His→Gln still shows efficient decarboxylation activity in* $CYP450_{OleT}$. The MD simulation of the H85Q mutant of $CYP450_{OleT}$ shows that in the absence of the histidine at 85th position, an Asp239 plays a similar role via a well-organized water channel. Our simulation shows that such a water channel is vital for the optimal substrate positioning needed for the decarboxylation activity and is gated by the Q85-R242 residue pair. Interestingly, the MD simulation of the WT $CYP450_{BS\beta}$ shows a closed channel that blocks the access to the Glu236 (analogous residue to Asp239 in $CYP450_{OleT}$) and, therefore $CYP450_{BS\beta}$ shows low decarboxylation activity.

1. Introduction:

Cytochrome P450 (CYP450) is a superfamily of heme-dependent enzymes with members present in almost every living creature.[1–3] These enzymes are capable of catalyzing a wide variety of endogenous and exogenous organic substrates by utilizing molecular oxygen.[4–10] The catalytic reaction is controlled by well-organized machinery which is triggered by the entry of the substrate into the active site.[11,12] The active oxidants and different catalytic cycles, which are involved in this process are well documented in several reviews and monographs.[8–12] In contrast to the oxygen-consuming CYP450s, which require two protons and two electrons from water/acid and a reducing partner to generate the active species Compound I (Cpd I), the sub-family of CYP peroxygenases (CYP152) utilizes hydrogen peroxide (H_2O_2) to generate directly the active species Cpd I (cf. Scheme 1).[13] The early discovered members of the peroxygenase family, $CYP450_{SP\alpha}$ and $CYP450_{BS\beta}$, are known to catalyze the hydroxylation of fatty acid substrates at α and β-positions, respectively.[14,15] However, the new member of the family, $CYP450_{OleT}$, produces terminal olefins via unusual decarboxylation of fatty acids.[16] Since terminal olefins are potentially useful as biofuels, several experimental and computational studies were performed to investigate the mechanism of the decarboxylation activity of $CYP450_{OleT}$.[17–26]

Interestingly, various investigations have led to inconclusive understanding of novel reactivity pattern. Thus, site-directed mutagenesis by Fang et al[27] showed that the mutation of Histidine at the 85th position of $CYP450_{OleT}$ resulted in insignificant alkene production or no decarboxylation activity. In a recent theoretical study, we have shown that H85 in $CYP450_{OleT}$ generates a polar environment favoring the decarboxylation activity by stabilizing the Cpd II intermediate i.e., hydroxy-Fe (IV).[28] In addition, it was found that His85 was responsible for the proton delivery to the post-decarboxylation intermediate, Cpd II (Fe-OH), and hence for resetting

the catalytic cycle for the next turnover. By comparison, $P450_{BS\beta}$, another member of the peroxygenase enzyme wherein Glutamine occupies the 85th position, gave a minor decarboxylation route alongside the major hydroxylation process. However, the Q85H mutation of the wild type (WT) $CYP450_{BS\beta}$ enzyme resulted in increased decarboxylation activity,[29] and as such, supported the important role of histidine 85 in steering the decarboxylation reaction in peroxygenases. A seemingly conflicting result was reported in 2017, by Matthews and their co-workers who found that the H85Q mutant in $P450_{OleT}$ produces a significant amount of alkene for various fatty acids.[30] The above reactivity patterns raise the following mechanistically intriguing questions:

(a) If both, the WT enzyme $CYP450_{BS\beta}$ and the H85Q mutant of $CYP450_{OleT}$, exhibit similar active site residues and substrate binding sites (cf. Fig 1), why then *the WT $CYP450_{BS\beta}$ prefers hydroxylation, whereas the H85Q mutant of $CYP450_{OleT}$ prefers decarboxylation?*

(b) Likewise, w*hat will be the alternative residue to H85 that will stabilize Cpd II, and how will the resting state be restored for the next catalytic turnover in the absence of the proton-donating residue histidine?*

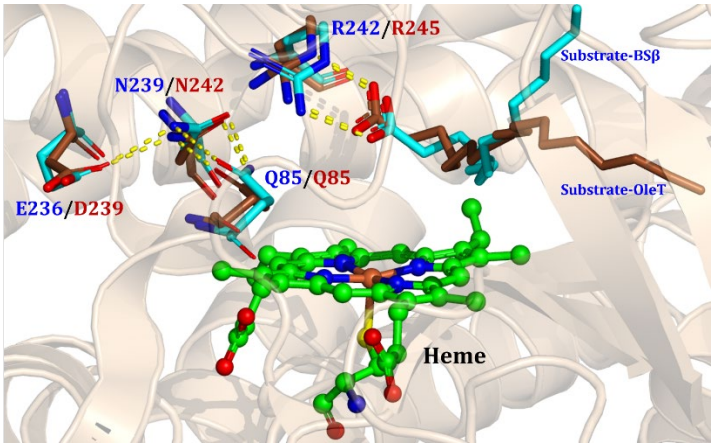

Figure 1. Overlaid crystal structures of the H85Q mutant of $CYP450_{OleT}$ (PDB code: 5M0O)[30], and the WT $CYP450_{BS\beta}$ (PDB code: 1IZO)[15]. Note that all the key residues in the two enzyme occupy the same positions. The residue color code for H85Q mutant of $CYP450_{OleT}$ is brown, while for WT $CYP450_{BS\beta}$ it is cyan.

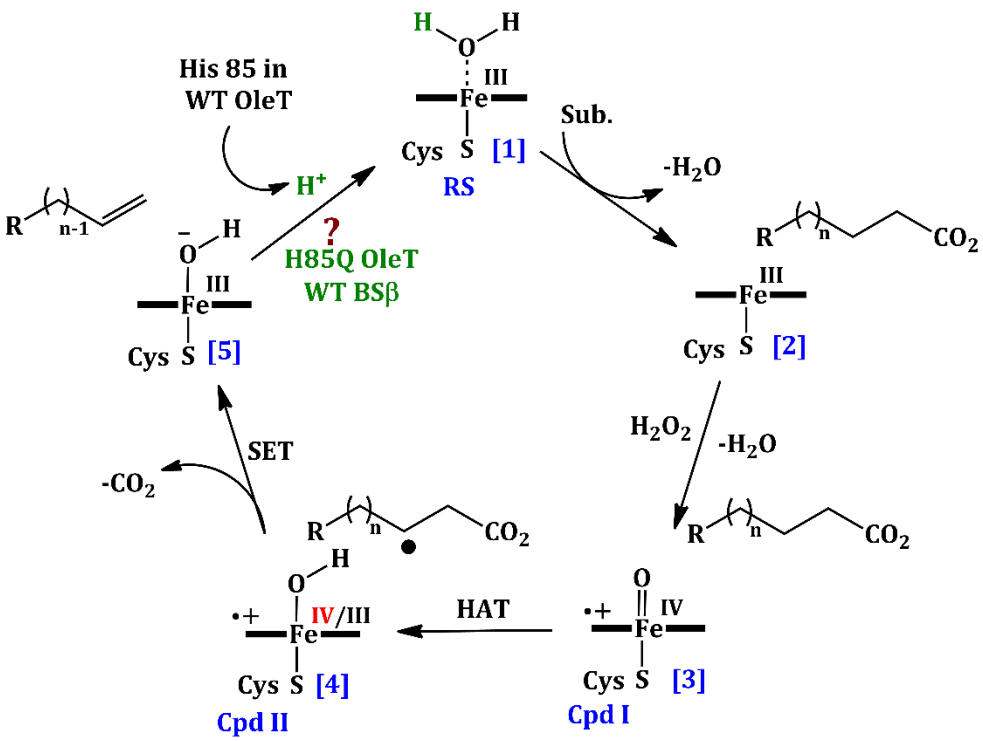

Scheme 1: Catalytic cycle of decarboxylation in $CYP450_{OleT}$. Note that, after decarboxylation, it is H85 that donates a proton and converts heme (*5*) to a resting state. (*1*). Whereas, in the H85Q $CYP450_{OleT}$ mutant, and WT $CYP450_{BS\beta}$ the protonation source that restores the resting state remains a mystery.

The present study responds to these queries using classical molecular dynamics (MD) simulation followed by QM/MM calculations for the H85Q mutant of $CYP450_{OleT}$ and WT $CYP450_{BS\beta}$. Our study shows an unprecedented gating mechanism *in the H85Q $CYP450_{OleT}$ mutant that allows the entry of an excessive amount of water molecules and prefers thereby decarboxylation. In addition, this controlled gating is key to the precise positioning that prefers decarboxylation of the substrate.*

2. Computational Details

2.1. System Preparation: Initial coordinates for the geometry of the enzyme have been taken from the fatty acid-bound crystal structures of H85Q mutant of $CYP450_{OleT}$ and WT $CYP450_{BS\beta}$ (respective PDBs are: 5M0O[30] and 1IZO[15]). Missing Hydrogen atoms in the protein residues were

added using the LEAP module of the AMBER 20 package employing the FF19SB[31] force field. Protonation states of the amino acids were estimated by PROPKA3.[32] The pKa of D239 was ~4.66; However, we used protonated D237 since it has been proposed to be a proton donor in this study. Necessary parameters for the ligand moiety were prepared by an antechamber module using the GAFF2 force field of Amber20. Partial atomic charges of the ligand were obtained by use of the RESP charge fitting method, calculated at HF/6-31G(d) level of theory.[33,34] The Force field for the Cpd I species was taken from already published parameters by Cheatham and co-workers.[35] The resulting system was then solvated in an octahedral box of TIP3P[36] waters extending up to 10Å off the protein surface. Subsequently, a few Na^+ ions were added to make our system electrically neutral.

2.2. MD Simulation:

After proper parametrization, the system was subject to minimization which removes poor contacts and geometrically-relaxes the system. This minimization was done by 5000 steps of steepest descent followed by 5000 steps of conjugate gradient approach. To adjust the temperature, the system was gently annealed for 50ps under NVT ensemble where constraints have been applied on the protein. Subsequently, density equilibration was performed for 1ns under NPT ensemble (constant temperature 300K and constant pressure of 1.0 atm). To maintain the constant temperature and pressure, we applied the Langevin thermostat[37] with a collision frequency of 2 ps and the Berendsen barostat[38] with a pressure relaxation time of 1 ps. This 1 ns density equilibration requires an MD simulation with weak restraints under periodic boundary conditions, which are applied until the system obtained a uniform density. Having a uniform density, all restraints which were applied before (during heating and density equilibration) have been removed. Then the system was further equilibrated for 3ns, followed by 100ns of production MD run. All simulations

were performed in three replicas starting from different initial velocities, each for 100ns. Hydrogen atoms were constrained using the SHAKE[39] algorithm, and particle mesh Ewald (PME)[40] was used to treat long range electrostatic interactions. All the simulations used the GPU version of the AMBER20 package.[41] The trajectory which resulted from the production run was used for analysis, using the CPPTRAJ[42] module of amber package. The visualization of the trajectory was done by VMD[43] software and PYMOL was used for the figure preparation.

2.3. QM/MM Calculations:

The reaction mechanism was investigated by QM/MM calculations performed on the representative snapshots taken from the MD trajectory. Calculations were carried out by ChemShell[44,45] employing Turbomole[46] for the QM part, and DL_POLY[47,48] using the FF19SB[31] Amber force field for MM the part. Asp239 was used for investigating the deprotonation feasibility in the H85Q mutant of $CYP450_{OleT}$. As such, the QM region contained the Heme, the substrate binding residue Arg245, the substrate, and all the water molecule that connect Asp239 to Heme. To account for the effect of the environment, we considered as '*active region*' during the QM/MM calculations, all the protein residues and water molecules present up to 10 Å of the Heme surface. The atoms of this active region interact with the QM atoms and lead to subsequent polarization effects through electrostatic and van der Waals interactions. An electronic embedding scheme was used to account for the polarizing effect of the protein residues on the QM region. The hydrogen-linked atom with the charge shift model was applied to treat the atoms present at the boundary surface of the QM region and MM region.

QM/MM geometry optimization: The QM region was computed by use of the UB3LYP functional with two basis sets. For geometry optimization, potential energy surface scanning, and frequency calculations, we used the all electron basis set def2-SVP (henceforth, B1). The transition

states (TSs) were located by relaxed potential energy surface scans followed by full TS optimizations using the partitioned rational function optimization (P-RFO)[49] method implemented in the HDLC code. The zero-point energy was calculated for all the species, and all the final energies are reported at the UB3LYP/B1-D3+ZPE level**.** Energies at a higher basis set UB3LYP/def2-TZVP+ ZPE are documented in Tables S1 and S2 of the SI.

3. Results and Discussion

3.1. The Active Site Conformation for Decarboxylation:

To investigate the potential role of the active site conformation on the different catalytic activity, we performed several MD simulations with the H85Q mutant of $CYP450_{OleT}$ and the WT $CYP450_{BS\beta}$. During the simulations of both enzymes, we observed that the carboxylate end of the substrate persistently interacts with the guanidinium groups of Arg245/242 (in $CYP450_{OleT}$/$CYP450_{BS\beta}$). However, the positioning of the substrates was significantly different in both enzymes as shown in Figures 2A and 2B:

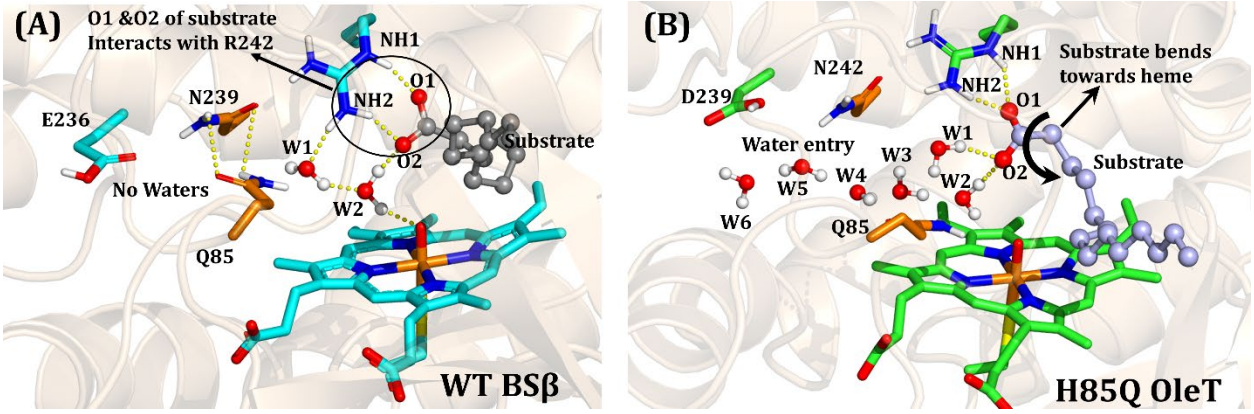

Figure 2. Conformational comparison of WT $CYP450_{BS\beta}$ and H85Q $CYP450_{OleT}$ mutant: **(A)** WT $CYP450_{BS\beta}$**.** Note the closed-gate conformation due to the Q85-N239 interaction near the active site which blocks the water access. **(B)** The H85Q mutant of $CYP450_{OleT.}$ Note the open-gate conformation due to loss of the Q85-N242 interaction which allows plenty of water connecting through D239.

Thus, in the WT $CYP450_{BS\beta}$ enzyme, both oxygen atoms of the carboxylate group interact with the amino hydrogens of Arg242 (cf. Figure 2A). On the other hand, in the H85Q mutant of $CYP450_{OleT}$, just one carboxylate oxygen (O1) interacts with the guanidium group of Arg245. In contrast, the other oxygen (O2) interacts with nearby water molecules (w1 and w2). The interaction of O2 with the water molecules pulls the carboxylate end of the substrate towards the Heme. This orientation of the substrate is *exactly the same* as was found originally[28] in the WT $CYP450_{OleT}$ (where a similar carboxylate bending was observed, due to the interaction of the substrate with H85 via a water molecule and only one carboxylate oxygen maintained interaction with Arg245). It is noteworthy that WT $CYP450_{OleT}$ exhibits decarboxylation activity predominantly; hence, we may conclude that the *precise positioning of the substrate molecule due to an additional proton channel causes decarboxylation activity in both the $CYP450_{OleT}$ and its H85Q variant.*

This, however, creates another mechanistic question: in the WT $CYP450_{OleT}$ the Histidine 85 residue provides a water-mediated proton source, so what is the alternative source of proton in the H85Q mutant of $P450_{OleT}$? To answer these questions, we thoroughly monitored the protein topology in the WT $P450_{BS\beta}$ and H85Q mutant of $P450_{OleT}$.

Interestingly, during the simulation of the H85Q mutant $CYP450_{OleT}$ vis-à-vis WT $CYP450_{BS\beta}$, we observe a significant difference in the interactions of Gln85 with Asn242/Asn239 (in $CYP450_{OleT}$/ $CYP450_{BS\beta}$) and in the water occupancy (cf. Fig 3B). This difference is apparent by inspection of the distance plots in Figures 3A and 3B. As can be seen, the Q85—N242 distance in the mutant of $CYP450_{OleT}$ increases significantly and becomes ~7Å with the course of the simulation (black line in Figure 3A). Due to the increased Q85—N242 distance, a doorway opens that regulates the flow of an organized water channel (W2-W3-W4-W5) stretching through the

heme, substrate, and the acidic Asp239 residue, as pointed out above in Figure 2. This water channel (the red channel in Figure 3C) is very persistent throughout the simulation (see supplementary video VS1) and can be verified by the increased water population in Figure 3B (black lines). In addition, the finding of a similar "open doorway" conformation with an extended water network in *in-silico* mutated (H85Q) $CYP450_{OleT}$ with a different substrate (arachidonic acid) generalizes this observation (cf. Fig S1). However, the same Q85—N239 distance remains close in WT $CYP450_{BS\beta}$ (red lines in Figure 3A), which in turn closes the 'doorway' and blocks the water chain (note the smaller population of water molecules in the red lines in Figure 3B, and no water channel in WT $P450_{BS\beta}$). The positioning of Q85-N242/N239 residue in mutant $CYP450_{OleT}$ and WT $CYP450_{BS\beta}$ at different time frames can be seen in Figure S2 in SI and supplementary video VS1 and VS2.

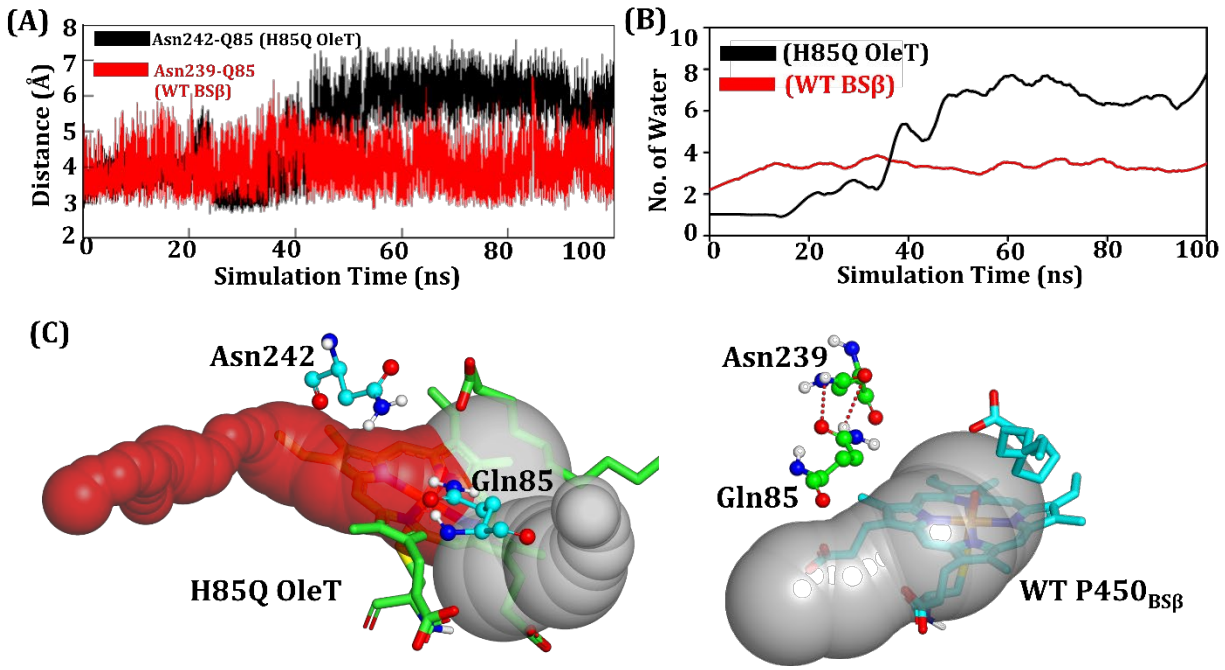

Figure 3. A) Distance between Q85 and N242/239 residue in the $P450_{OleT}$ mutant vis-à-vis the WT $P450_{BS\beta}$ enzyme. Note that the Q85—N239 distance is shorter in WT $CYP450_{BS\beta}$ than the Q85—N242 distance in the H85Q mutant of $CYP450_{OleT}$. (B) Water occupancy within 5 Å of Asn242/239 in H85Q $CYP450_{OleT}$ (in black) and WT $CYP450_{BS\beta}$ (in red). C) A comparison of

water channels in the H85Q mutant $P450_{OleT}$ and WT $P450_{BS\beta}$. Note the new prominent water channel (red) formed between Asn242 and Gln85 in the H85Q mutant of $P450_{OleT,}$ which is blocked due to close interaction in WT $P450_{BS\beta}$.

In a nutshell, therefore, in the H85Q mutant of $CYP450_{OleT,}$ an organized water channel (that connects Asp239 to oxo-iron via the substrate) acts during decarboxylation as a proton donor to the heme (state 5, Scheme 1). As such, the heme is able to achieve its resting state, much as in the WT $CYP450_{OleT}$.

3.2. The Protonation of state 5

To check the feasibility of the proton donation from Asp239, let us discuss the QM/MM calculations for the following steps in the cycle (Scheme 1): Step 4 (Cpd II) → Step 5, and Step 5→ resting state. The first step, step 4 (Cpd II) → Step 5, corresponds to the decarboxylation of the substrate which proceeds easily with an energy barrier of 4.1 kcal/mol (cf. Fig 4). The next step, Step 5→ resting state, involves the protonation of the Fe-(OH) and restoration of the resting state which is a condition for an efficient catalytic turnover. In $P450_{OleT}$ this is achieved by the His85 residue[28], however, in the absence of His85 (i.e., H85Q mutant of $P450_{OleT}$ and $P450_{BS\beta}$, we propose two possible mechanisms using QM/MM calculations, pathways 1 and 2 in Figure 4.

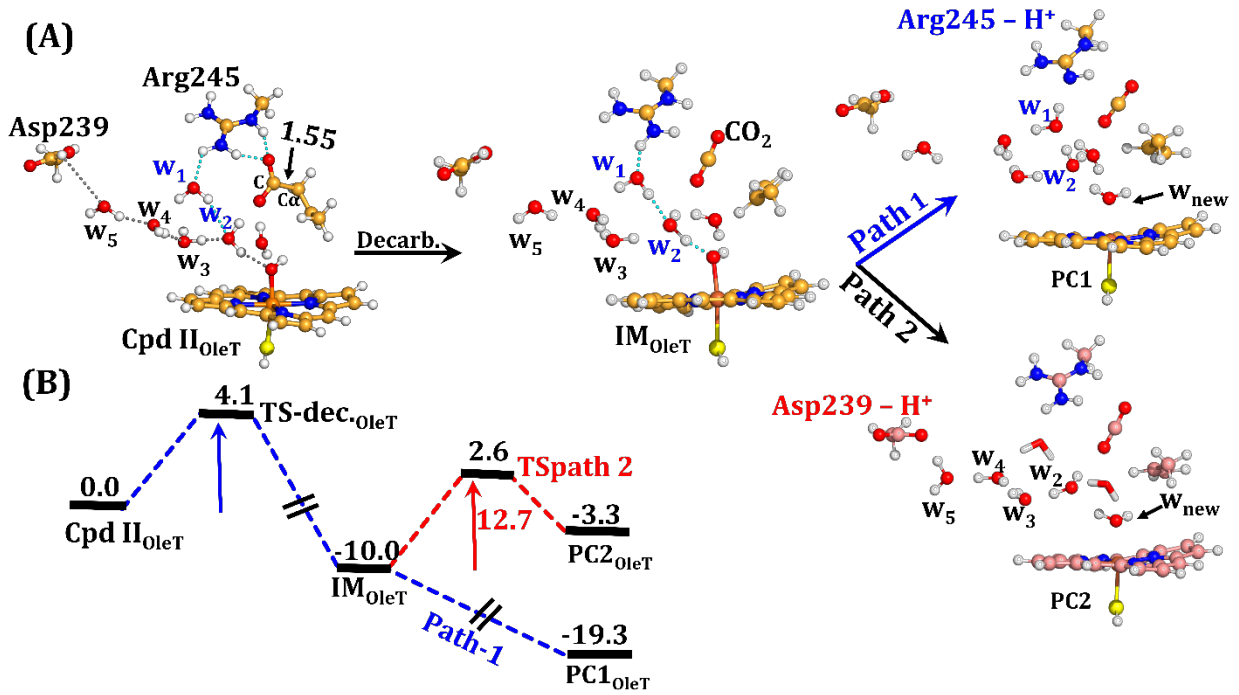

Figure 4. QM/MM/B3LYP-D3/def2-SVP calculated decarboxylation mechanism in H85Q mutant of CYP450$_{OleT}$. (A) Geometries (shown in ball and stick) observed during the PES scanning of decarboxylation reaction. The reported energy values are in kcal/mol. Note that after decarboxylation, the intermediate IM$_{OleT}$ may restore the resting state via two pathways 1 and 2. Transition state structures involved in the reaction profile are incorporated in the SI (cf Fig S3).

Pathway 1: The QM/MM for this pathway is shown in Figure 4A, where Arg245 donates a proton to IM$_{MUT\text{-}OleT}$ (state 5) and resets the catalytic cycle. Thus, the positively charged Arg245 (for charges cf. Table S3) easily transfers its proton to the negatively charged IM$_{MUT\text{-}OleT}$ (charge= −0.66), using a barrier-free Grotthuss type mechanism, via water molecules W1 and W2. In the next step, the deprotonated Arg245 will accept a proton from Asp239 via an organized water chain and restores its state which will start the next round of the catalytic cycle. A protonation mechanism of Arg245 through Asp239 is shown in SI (cf FigS4).

Pathway 2: In this pathway, Asp239 directly donates its proton to IM$_{OleT}$ (state 5) via a well-organized water chain W2-W3-W4-W5. The energy barrier for this pathway (12.7 kcal/mol) is also rather small, such that this route constitutes a feasible mechanism as well. However, the

barrier-free pathway is definitely preferable. Clearly, therefore, Asp239 plays a major role as a director of an excessive amount of water molecules into the active site, while at the same time, the interaction of the substrate with the nearby water molecules stretches the carboxylate towards the heme and eases the decarboxylation.

Therefore, our QM/MM calculation provides solid evidence that Arg245 or Asp239 may serve as a proton donating sources to the heme in the H85Q mutant of $CYP450_{OleT}$, and thereby play the same function as H85 (in WT) in restoring the resting state.

Since also WT $CYP450_{BS\beta}$ exhibits some decarboxylation activity, we propose that it also follows a similar route to Pathway 1. The explicit QM/MM study of WT $CYP450_{BS\beta}$ in Figure 5 validates this mechanism (cf. Fig S5, S6 and Table S2, S4). Interestingly, by comparison to the $CYP450_{OleT}$ mutant, the decarboxylation, as well as protonation from the Arg242 residue in WT $CYP450_{BS\beta}$, were found to have substantial energy barriers, i.e., 14.3/3.5 kcal/mol, respectively. This difference in the barriers vs. the barrier-free option 1 is due to different organizations of the water gateway (open in $CYP450_{OleT\text{-}MUT}$ vs. close in $CYP450_{BS\beta\text{-}WT}$). In addition, the substantial barrier in WT $CYP450_{BS\beta}$ matches the observation of less decarboxylation activity of this enzyme.

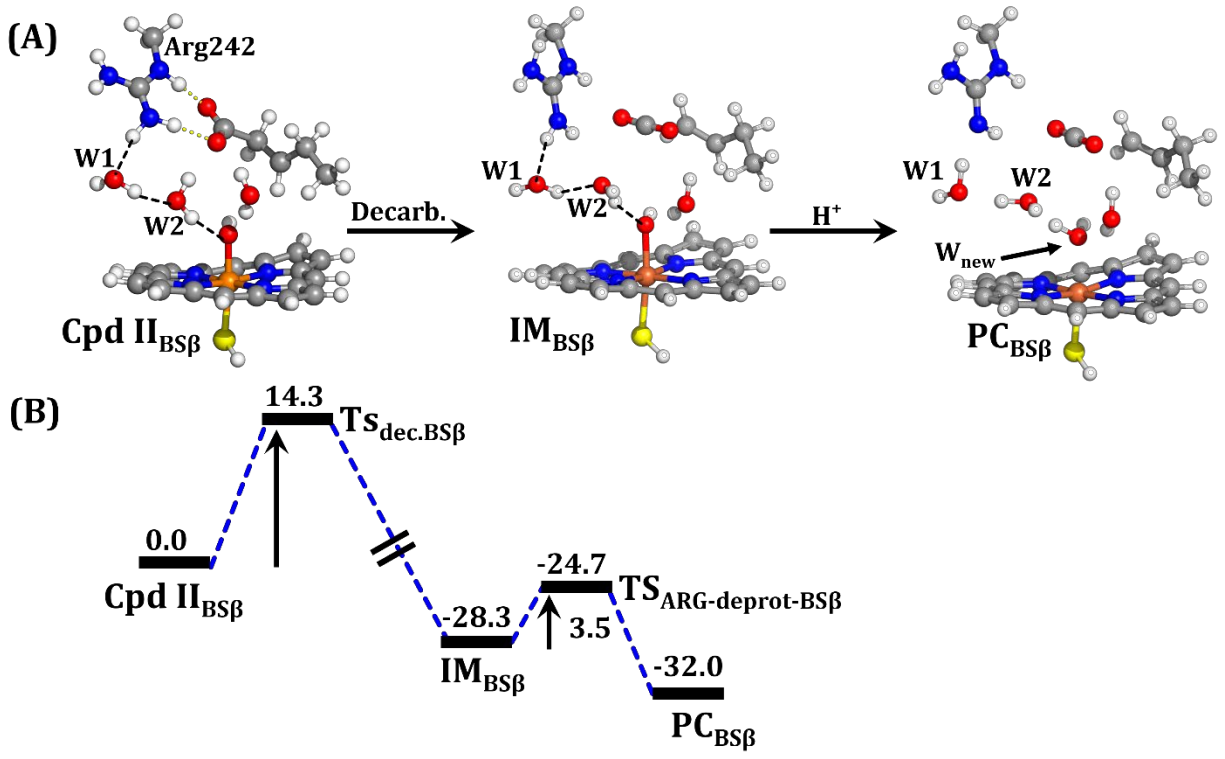

Figure 5. (A) QM/MM observed geometries (in the ball and stick model) observed during PES scanning for the decarboxylation reaction in WT CYP450$_{BS\beta}$. **(B)** Corresponding energy profile calculated at QM/MM/B3LYP-D3/def2-SVP level of theory. All energies are in kcal/mol. Transition state structures involved in the reaction profile are incorporated in SI (cf Fig S5).

4. Conclusion:

Our study reveals that even though H85Q variant of CYP450$_{OleT}$ and WT CYP450$_{BS\beta}$ enzymes consist of the same active site (cf Fig 1), their different conformations (Open-door in the H85Q mutant CYP450$_{OleT}$ and completely closed-door in WT CYP450$_{BS\beta}$ are responsible for the observed favorable decarboxylation of the H85Q CYP450$_{OleT}$ mutant vis-à-vis WT CYP450$_{BS\beta}$.

Nevertheless, our MD simulation and QM/MM calculations show that the two enzymes follow similar mechanisms for the decarboxylation reaction, as depicted in Scheme 2. Thus, as soon as the bond between C-Cα gets broken, the fatty acid substrate gets converted into a neutral

terminal alkene followed by CO_2 liberation. Since now the neutral products (alkene and CO_2) no longer interact with the positively charged Arg245/Arg242 (OleT/BSβ), these residues immediately protonate Fe(III)OH$^-$ species and reset the catalytic cycle for the next turnover.

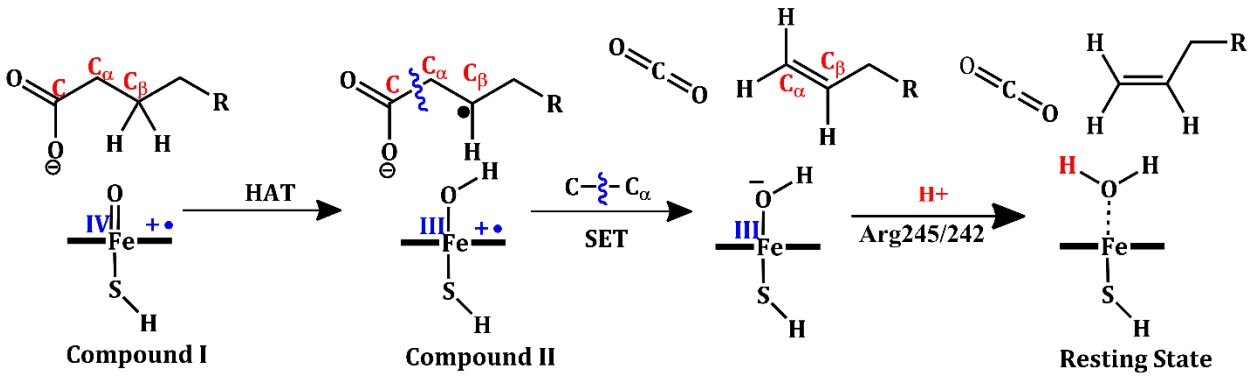

Scheme 2. QM/MM studied reaction profile for the decarboxylation reaction in the H85Q mutant of $CYP450_{OleT}$ and WT $CYP450_{BS\beta}$.

5. Acknowledgements: KDD acknowledges Department of Biotechnology, Ministry of Science and Technology, Govt. of India for Ramalingaswami Re-entry research grant (BT/Re-entry/RLF/10/2017). SS is supported by the ISF (grant 520/18).

6. Corresponding Author Details:

1. Prof. Sason Shaik, sason.shaik@gmail.com, sason@yfaat.ch.huji.ac.il, ORCID: 0000-0001-7643-9421

2. Dr. Kshatresh Dutta Dubey, kshatresh@gmail.com, kshatresh.dubey@snu.edu.in, ORCID: 0000-0001-8865-7602

7. Supplementary Materials:

The Supporting Information is available free of charge on the ACS Publications website at http://pubs.acs.org. It contains the coordinates for the QM region for different reactive species, charge and spin densities, reaction profiles etc.

8. References:

(1) Oritz de Montellano, P. R. Cytochrome P-450. *Struct. Mech. Biochem.* **1995**.

(2) Sono, M.; Roach, M. P.; Coulter, E. D.; Dawson, J. H. Heme-Containing Oxygenases. *Chem. Rev.* **1996**, *96*, 2841–2888.

(3) Denisov, I. G.; Makris, T. M.; Sligar, S. G.; Schlichting, I. Structure and Chemistry of Cytochrome P450. *Chem. Rev.* **2005**, *105*, 2253–2278.

(4) Ortiz de Montellano, P. R. Hydrocarbon Hydroxylation by Cytochrome P450 Enzymes. *Chem. Rev.* **2010**, *110*, 932–948.

(5) Groves, J. T. Using Push to Get Pull. *Nat. Chem.* **2014**, *6*, 89–91.

(6) van Eldik, R. Introduction: Inorganic and Bioinorganic Mechanisms. *Chem. Rev.* **2005,** *105,* 1917-1922.

(7) Groves, J. T. Key Elements of the Chemistry of Cytochrome P-450: The Oxygen Rebound Mechanism. *Chem. Eduuc.* **1985,** *62,* 928-931.

(8) Meunier, B.; De Visser, S. P.; Shaik, S. Mechanism of Oxidation Reactions Catalyzed by Cytochrome P450 Enzymes. *Chem. Rev.* **2004**, *104*, 3947–3980.

(9) Shaik, S.; Kumar, D.; de Visser, S. P.; Altun, A.; Thiel, W. Theoretical Perspective on the Structure and Mechanism of Cytochrome P450 Enzymes. *Chem. Rev.* **2005**, *105*, 2279–2328.

(10) Shaik, S.; Cohen, S.; Wang, Y.; Chen, H.; Kumar, D.; Thiel, W. P450 Enzymes: Their Structure, Reactivity, and Selectivity□Modeled by QM/MM Calculations. *Chem. Rev.* **2010**, *110*, 949–1017.

(11) Dubey, K. D.; Shaik, S. Cytochrome P450—the Wonderful Nanomachine Revealed through Dynamic Simulations of the Catalytic Cycle. *Acc. Chem. Res.* **2019**, *52*, 389–399.

(12) Shaik, S.; Dubey, K. D. The Catalytic Cycle of Cytochrome P450: A Fascinating Choreography. *Trends Chem.* **2021**, *3*, 1027–1044.

(13) Munro, A. W.; McLean, K. J.; Grant, J. L.; Makris, T. M. Structure and Function of the Cytochrome P450 Peroxygenase Enzymes. *Biochem. Soc. Trans.* **2018**, *46*, 183–196.

(14) Fujishiro, T.; Shoji, O.; Nagano, S.; Sugimoto, H.; Shiro, Y.; Watanabe, Y. Crystal Structure of H2O2-Dependent Cytochrome P450SPα with Its Bound Fatty Acid Substrate: Insight into the Regioselective Hydroxylation of Fatty Acids at the α Position. *J. Biol. Chem.* **2011**, *286*, 29941–29950.

(15) Lee, D.-S.; Yamada, A.; Sugimoto, H.; Matsunaga, I.; Ogura, H.; Ichihara, K.; Adachi, S.; Park, S.-Y.; Shiro, Y. Substrate Recognition and Molecular Mechanism of Fatty Acid Hydroxylation by Cytochrome P450 from Bacillus Subtilis: Crystallographic, Spectroscopic, and Mutational Studies. *J. Biol. Chem.* **2003**, *278*, 9761–9767.

(16) Belcher, J.; McLean, K. J.; Matthews, S.; Woodward, L. S.; Fisher, K.; Rigby, S. E. J.; Nelson, D. R.; Potts, D.; Baynham, M. T.; Parker, D. A. Structure and Biochemical Properties of the Alkene Producing Cytochrome P450 OleTJE (CYP152L1) from the Jeotgalicoccus Sp. 8456 Bacterium. *J. Biol. Chem.* **2014**, *289*, 6535–6550.

(17) Chowdhury, A. S.; Ali, H. S.; Faponle, A. S.; De Visser, S. P. How External Perturbations Affect the Chemoselectivity of Substrate Activation by Cytochrome P450 OleTJE. *Phys. Chem. Chem. Phys.* **2020**, *22*, 27178–27190.

(18) Wang, Y.; Lan, D.; Durrani, R.; Hollmann, F. Peroxygenases En Route to Becoming Dream Catalysts. What Are the Opportunities and Challenges? *Curr. Opin. Chem. Biol.* **2017**, *37*, 1–9.

(19) Hsieh, C. H.; Huang, X.; Amaya, J. A.; Rutland, C. D.; Keys, C. L.; Groves, J. T.; Austin, R. N.; Makris, T. M. The Enigmatic P450 Decarboxylase OleT Is Capable of, but Evolved to Frustrate, Oxygen Rebound Chemistry. *Biochemistry* **2017**, *56*, 3347–3357.

(20) Faponle, A. S.; Quesne, M. G.; De Visser, S. P. Origin of the Regioselective Fatty-Acid Hydroxylation versus Decarboxylation by a Cytochrome P450 Peroxygenase: What Drives the Reaction to Biofuel Production? *Chem. - A Eur. J.* **2016**, *22*, 5478–5483.

(21) Dennig, A.; Kuhn, M.; Tassoti, S.; Thiessenhusen, A.; Gilch, S.; Bülter, T.; Haas, T.; Hall, M.; Faber, K. Oxidative Decarboxylation of Short-Chain Fatty Acids to 1-Alkenes. *Angew. Chemie - Int. Ed.* **2015**, *54*, 8819–8822.

(22) Zachos, I.; Gaßmeyer, S. K.; Bauer, D.; Sieber, V.; Hollmann, F.; Kourist, R. Photobiocatalytic Decarboxylation for Olefin Synthesis. *Chem. Commun.* **2015**, *51*, 1918–1921.

(23) Lin, F. M.; Marsh, E. N. G.; Lin, X. N. Recent Progress in Hydrocarbon Biofuel Synthesis: Pathways and Enzymes. *Chinese Chem. Lett.* **2015**, *26*, 431–434.

(24) Grant, J. L.; Hsieh, C. H.; Makris, T. M. Decarboxylation of Fatty Acids to Terminal Alkenes by Cytochrome P450 Compound I. *J. Am. Chem. Soc.* **2015**, *137*, 4940–4943.

(25) Liu, Y.; Wang, C.; Yan, J.; Zhang, W.; Guan, W.; Lu, X.; Li, S. Hydrogen Peroxide-Independent Production of α-Alkenes by OleT JE P450 Fatty Acid Decarboxylase.

Biotechnol. Biofuels **2014**, *7*, 1–12.

(26) Cantú Reinhard, F. G.; Lin, Y.-T.; Stańczak, A.; de Visser, S. P. Bioengineering of Cytochrome P450 OleTJE: How Does Substrate Positioning Affect the Product Distributions? *Molecules* **2020**, *25*, 2675.

(27) Fang, B.; Xu, H.; Liu, Y.; Qi, F.; Zhang, W.; Chen, H.; Wang, C.; Wang, Y.; Yang, W.; Li, S. Mutagenesis and Redox Partners Analysis of the P450 Fatty Acid Decarboxylase OleT JE. *Sci. Rep.* **2017**, *7*, 1–7.

(28) Yadav, S.; Shaik, S.; Siddiqui, S. A.; Kalita, S.; Dubey, K. D. Local Electric Fields Dictate Function: The Different Product Selectivities Observed for Fatty Acid Oxidation by Two Deceptively Very Similar P450-Peroxygenases OleT and BSβ. *J. Chem. Inf. Model.* **2022**, *62*, 1025–1035.

(29) Rude, M. A.; Baron, T. S.; Brubaker, S.; Alibhai, M.; Del Cardayre, S. B.; Schirmer, A. Terminal Olefin (1-Alkene) Biosynthesis by a Novel P450 Fatty Acid Decarboxylase from Jeotgalicoccus Species. *Appl. Environ. Microbiol.* **2011**, *77*, 1718–1727.

(30) Matthews, S.; Belcher, J. D.; Tee, K. L.; Girvan, H. M.; McLean, K. J.; Rigby, S. E. J.; Levy, C. W.; Leys, D.; Parker, D. A.; Blankley, R. T.; Munro, A. W. Catalytic Determinants of Alkene Production by the Cytochrome P450 Peroxygenase OleTJE. *J. Biol. Chem.* **2017**, *292*, 5128–5143.

(31) Tian, C.; Kasavajhala, K.; A. A. Belfon, K.; Raguette, L.; Huang, H.; N. Migues, A.; Bickel, J.; Wang, Y.; Pincay, J.; Wu, Q.; Simmerling, C. Ff19SB: Amino-Acid-Specific Protein Backbone Parameters Trained against Quantum Mechanics Energy Surfaces in Solution. *J. Chem. Theory Comput.* **2019**, *16*, 528–552.

(32) Olsson, M. H. M.; Søndergaard, C. R.; Rostkowski, M.; Jensen, J. H. PROPKA3: Consistent Treatment of Internal and Surface Residues in Empirical p K a Predictions. *J. Chem. Theory Comput.* **2011**, *7*, 525–537.

(33) Cornell, W. D.; Cieplak, P.; Bayly, C. I.; Kollman, P. A. Application of RESP Charges to Calculate Conformational Energies, Hydrogen Bond Energies, and Free Energies of Solvation. *J. Am. Chem. Soc.* **2002**, *115*, 9620–9631.

(34) Bayly, C. I.; Cieplak, P.; Cornell, W.; Kollman, P. A. A Well-Behaved Electrostatic Potential Based Method Using Charge Restraints for Deriving Atomic Charges: The RESP Model. *J. Phys. Chem.* **1993**, *97*, 10269–10280.

(35) Shahrokh, K.; Orendt, A.; Yost, G. S.; Cheatham III, T. E. Quantum Mechanically Derived AMBER-compatible Heme Parameters for Various States of the Cytochrome P450 Catalytic Cycle. *J. Comput. Chem.* **2012**, *33*, 119–133.

(36) Jorgensen, W. L.; Chandrasekhar, J.; Madura, J. D.; Impey, R. W.; Klein, M. L. Comparison of Simple Potential Functions for Simulating Liquid Water. *J. Chem. Phys.* **1983**, *79*, 926–935.

(37) Izaguirre, J. A.; Catarello, D. P.; Wozniak, J. M.; Skeel, R. D. Langevin Stabilization of Molecular Dynamics. *J. Chem. Phys.* **2001**, *114*, 2090–2098.

(38) Berendsen, H. J. C.; Postma, J. P. M. van; Van Gunsteren, W. F.; DiNola, A.; Haak, J. R. Molecular Dynamics with Coupling to an External Bath. *J. Chem. Phys.* **1984**, *81*, 3684–3690.

(39) Ryckaert, J.-P.; Ciccotti, G.; Berendsen, H. J. C. Numerical Integration of the Cartesian

Equations of Motion of a System with Constraints: Molecular Dynamics of n-Alkanes. *J. Comput. Phys.* **1977**, *23*, 327–341.

(40) Darden, T.; York, D.; Pedersen, L. Particle Mesh Ewald: An N· Log (N) Method for Ewald Sums in Large Systems. *J. Chem. Phys.* **1993**, *98*, 10089–10092.

(41) Salomon-Ferrer, R.; Gotz, A. W.; Poole, D.; Le Grand, S.; Walker, R. C. Routine Microsecond Molecular Dynamics Simulations with AMBER on GPUs. 2. Explicit Solvent Particle Mesh Ewald. *J. Chem. Theory Comput.* **2013**, *9*, 3878–3888.

(42) Roe, D. R.; Cheatham III, T. E. PTRAJ and CPPTRAJ: Software for Processing and Analysis of Molecular Dynamics Trajectory Data. *J. Chem. Theory Comput.* **2013**, *9*, 3084–3095.

(43) Humphrey, W.; Dalke, A.; Schulten, K. VMD: Visual Molecular Dynamics. *J. Mol. Graph.* **1996**, *14*, 33–38.

(44) Metz, S.; Kästner, J.; Sokol, A. A.; Keal, T. W.; Sherwood, P. C Hem S Hell—a Modular Software Package for QM/MM Simulations. *Wiley Interdiscip. Rev. Comput. Mol. Sci.* **2014**, *4*, 101–110.

(45) Sherwood, P.; de Vries, A. H.; Guest, M. F.; Schreckenbach, G.; Catlow, C. R. A.; French, S. A.; Sokol, A. A.; Bromley, S. T.; Thiel, W.; Turner, A. J.; Billeter, S.; Terstegen, F.; Thiel, S.; Kendrick, J.; Rogers, S. C.; Casci, J.; Watson, M.; King, F.; Karlsen, E.; Sjøvoll, M.; Fahmi, A.; Schäfer, A.; Lennartz, C. QUASI: A General Purpose Implementation of the QM/MM Approach and Its Application to Problems in Catalysis. *J. Mol. Struct. THEOCHEM* **2003**, *632*, 1–28.

(46) Balasubramani, S. G.; Chen, G. P.; Coriani, S.; Diedenhofen, M.; Frank, M. S.; Franzke, Y. J.; Furche, F.; Grotjahn, R.; Harding, M. E.; Hättig, C. TURBOMOLE: Modular Program Suite for Ab Initio Quantum-Chemical and Condensed-Matter Simulations. *J. Chem. Phys.* **2020**, *152*, 184107.

(47) Smith, W.; Forester, T. R. DL_POLY_2.0: A General-Purpose Parallel Molecular Dynamics Simulation Package. *J. Mol. Graph.* **1996**, *14*, 136–141.

(48) Ahlrichs, R.; Bär, M.; Häser, M.; Horn, H.; Kölmel, C. Electronic Structure Calculations on Workstation Computers: The Program System Turbomole. *Chem. Phys. Lett.* **1989**, *162*, 165–169.

(49) Kästner, J.; Carr, J. M.; Keal, T. W.; Thiel, W.; Wander, A.; Sherwood, P. DL-FIND: An Open-Source Geometry Optimizer for Atomistic Simulations. *J. Phys. Chem. A* **2009**, *113*, 11856–11865.